

Crystalline electric field effects in $CeMIn_5$ ($M=Co,Rh,Ir$): Superconductivity and the influence of Kondo spin fluctuations

A. D. Christianson,^{1,2} E. D. Bauer,² J. M. Lawrence,¹ P. S. Riseborough,³ N. O. Moreno,² P. G. Pagliuso,² J. L. Sarrao,² J. D. Thompson,² E. A. Goremychkin,⁴ F. R. Trouw,² M. P. Hehlen,² and R. J. McQueeney^{2,5}

¹University of California, Irvine, California 92697, USA

²Los Alamos National Laboratory, Los Alamos, New Mexico 87545, USA

³Temple University, Philadelphia, Pennsylvania 19122, USA

⁴Argonne National Laboratory, Argonne, Illinois 60439, USA

⁵Iowa State University, Ames, Iowa 50011, USA

(Received 1 March 2004; revised manuscript received 29 May 2004; published 18 October 2004)

We have measured the crystalline electric field (CEF) excitations of the $CeMIn_5$ ($M=Co,Rh,Ir$) series of heavy fermion superconductors by means of inelastic neutron scattering. In each case, the CEF excitations are considerably broadened, due to Kondo hybridization of the localized f -moments with the conduction electrons. Fits to a phenomenological CEF model reproduce the inelastic neutron scattering spectra and the high-temperature magnetic susceptibility. We also present calculations within the noncrossing approximation (NCA) to the Anderson impurity model, including the effect of CEF level-splitting for the inelastic neutron scattering spectra and the magnetic susceptibility. Our results indicate that the CEF level-splitting in all three materials is similar, and can be thought of as being derived from the cubic parent compound $CeIn_3$ in which an excited state quartet at ~ 12 meV is split into two doublets by the lower symmetry of the tetragonal environment of the $CeMIn_5$ materials. The evolution of the superconducting transition temperatures in the different members of $CeMIn_5$ can be understood as a direct consequence of the strength of the $4f$ -conduction electron hybridization.

DOI: 10.1103/PhysRevB.70.134505

PACS number(s): 74.70.-b, 71.70.Ch, 78.70.Nx

I. INTRODUCTION

The discovery of the family of $CeMIn_5$ ($M=Co,Rh,Ir$) heavy Fermion superconductors has sparked great interest.¹⁻⁵ This is in large part due to the small number of heavy fermion superconductors available for study, the unusually high T_c (2.3 K) observed for $CeCoIn_5$,³ and the presence of superconductivity and magnetism in the same crystal structure. The substitution of different transition metals (Co, Rh, or Ir) affects the nearest neighbor environment of the Ce^{3+} ion both through small changes in the position of the neighboring ions and through differing hybridization of the Ce f -electron with the conduction electrons. This allows for a comparison among the different members of the family where many of the complicating effects normally encountered in the study of heavy fermion materials can be taken to be approximately the same.

All members of the $CeMIn_5$ family crystallize in the tetragonal $HoCoGa_5$ crystal structure (space group $P4/mmm$) and can be viewed structurally as being composed of alternating layers of $CeIn_3$ and MIn_2 . At ambient pressure, $CeCoIn_5$ and $CeIrIn_5$ are superconducting at 2.3³ and 0.4 K,² respectively. On the other hand, $CeRhIn_5$ undergoes an antiferromagnetic transition at 3.8 K and upon the application of pressure becomes superconducting at 2.1 K and 16 kbar coinciding with a suppression of the Néel order.¹ The origin of superconductivity in these materials remains poorly understood. However, there is substantial evidence of the unconventional nature of the superconductivity, including power-law behavior in the low temperature specific heat and thermal conductivity^{6,7} and the spin lattice relaxation rate.⁸⁻¹⁰

A prominent view of the origin of heavy Fermion superconductivity in the $CeMIn_5$ compounds is that they are in close proximity to a quantum critical point (QCP).¹¹⁻¹⁵ The substitution of one transition metal for another in this family changes the $4f$ -conduction electron hybridization in a manner analogous to the effect of applied pressure on $CeIn_3$.¹⁶ The Kondo temperature (T_K) increases from 5 K in $CeRhIn_5$ to 17 K in $CeCoIn_5$;²⁸ when the Kondo energy becomes sufficiently larger than the antiferromagnetic exchange an evolution to a nonmagnetic and superconducting state occurs. The strong magnetic fluctuations present near a QCP are then implicated as the analog to phonons in conventional BCS superconductivity.

Crystalline electric field (CEF) effects are important for the heavy fermion ground states in these materials. It has been argued that the symmetry of the ground state CEF doublet in these materials may be directly relevant to the f -conduction electron hybridization and in some cases may produce spin fluctuations which are more favorable to the formation of the superconducting condensate.¹⁷ In another proposal, CEF splitting affects the competition between spin and orbital fluctuations that, in turn, controls the ground state configuration.¹⁸ A number of attempts have been made based upon bulk measurements to elucidate the CEF splittings in the $CeMIn_5$ series^{17,19-22} but there are significant discrepancies in the reported results. To clarify the role of CEF excitations and to resolve the discrepancies found in previous experiments, we have performed inelastic neutron scattering (INS) experiments that directly probe the CEF excitations in the $CeMIn_5$ series. For Ce^{3+} in a tetragonal environment, the CEF Hamiltonian can be written as

TABLE I. Experimental incident energies and temperatures. E_i indicates the incident energy in meV and the numbers in brackets indicate the temperature of the measurement(s) at that incident energy. An * indicates that data for a nonmagnetic analog was collected under the same experimental conditions.

Material	Instrument	E_i [T]
CeRhIn ₅	LRMECS	15 [8, 100], 35 [8*, 70*, 100*, 140*], 50 [8], 60 [8, 100], 80 [8,100]
	PHAROS	16.6 [16*], 48.1 [16*]
CeCoIn ₅	LRMECS	35 [10*, 80, 150], 60 [10]
	PHAROS	30.2 [18], 48.5 [18, 80]
CeIrIn ₅	LRMECS	15 [10*], 30 [10*, 70*], 35 [10, 100], 50 [10, 100], 60 [10*], 80 [10, 100]
	PHAROS	30.2 [18*, 70]

$$H_{CEF} = B_2^0 O_2^0 + B_4^0 O_4^0 + B_4^4 O_4^4, \quad (1)$$

where the B_l^m are the CEF parameters and the O_l^m are the Stevens operator equivalents. Diagonalization of this Hamiltonian yields the following wave functions.²³

$$\Gamma_7^1 = \alpha \left| \pm \frac{5}{2} \right\rangle - \beta \left| \mp \frac{3}{2} \right\rangle, \quad \Gamma_7^2 = \beta \left| \pm \frac{5}{2} \right\rangle + \alpha \left| \mp \frac{3}{2} \right\rangle, \quad (2)$$

$$\Gamma_6 = \left| \pm \frac{1}{2} \right\rangle.$$

The energy levels are determined from the positions of the peaks in the INS spectra, while the mixing parameters (α and β) are determined from the ratios of the integrated weights of the peaks. The $4f$ -conduction electron hybridization that is responsible for the Kondo effect causes the CEF excitation energies to shift to higher energies and the linewidths to broaden by an amount proportional to $k_B T_K$. The linewidth of the quasielastic scattering within the groundstate doublet is essentially equal to the Kondo energy $k_B T_K$.

A commonly applied phenomenology for calculating the susceptibility treats the CEF levels as delta functions but adds a molecular field term λ to the CEF susceptibility χ_{CEF} so that $1/\chi_{tot} = 1/\chi_{CEF} + \lambda$. Such a term is often used to represent antiferromagnetic interactions $\lambda = \beta T_N / C_J$. When positive, it also can represent the Kondo effect at high temperatures where $\chi \rightarrow C_{5/2} / (T + \alpha T_K)$ (where $C_{5/2}$ is the $J=5/2$ Curie constant for Ce and $\alpha \sim 1$) so that $\lambda = \alpha T_K / C_J$. Such an *ad hoc* approach, cannot, however, capture the effect of Kondo scattering on the susceptibility and neutron spectra at low temperature. The Kondo effect *can* be treated consistently at all temperatures in a calculation of the CEF scattering and the magnetic susceptibility that includes the CEF energies and mixing parameters in the Anderson impurity model. Of course, neither of these approaches correctly treats the antiferromagnetic correlations and/or $4f$ lattice coherence that are expected at low temperatures in these compounds.

In the next section we give details of the experimental and theoretical techniques applied in this study. In Sec. III we present the INS spectra for the members $M = \text{Co, Ir, Rh}$ of the CeMIn_5 family and fits to the INS spectra and the magnetic

susceptibility using both the CEF phenomenology and Anderson model calculations. A discussion of error analysis, other determinations of the CEF level schemes, and the importance of CEF excitations to CeMIn_5 is given in Sec. IV. In Sec. V we summarize our results and conclusions.

II. EXPERIMENTAL AND THEORETICAL DETAILS

Large high quality single crystals of CeMIn_5 and the non-magnetic analogous LaMIn_5 were obtained using the flux-growth method.²⁴ For CeCoIn_5 and YCoIn_5 , polycrystalline samples were obtained by heating stoichiometric amounts of the constituent elements in an alumina crucible sealed within a quartz tube to 1100 °C, and cooling to 900 °C, and then quenching in liquid nitrogen. After the samples were annealed at 600 °C for 3 weeks, they were then etched in dilute HCl to remove excess free In. Subsequent magnetic susceptibility measurements indicated the free In content to be less than 2%.²⁵ The resulting samples were powdered and placed in a rigid flat plate aluminum sample holder. This sample geometry served to not only minimize the effect of the strong neutron absorption of Rh, Ir, and In but maintained a uniform sample distribution enabling an accurate absorption correction.

Inelastic neutron scattering experiments were performed on two inelastic chopper spectrometers: PHAROS at the Manuel Lujan Neutron Science Center (Los Alamos National Laboratory) and LRMECS at the Intense Pulsed Neutron Source (Argonne National Laboratory). The experimental configuration of LRMECS is the same as described previously.²⁶ The experimental configuration of PHAROS is similar to LRMECS but with the notable exceptions of position sensitive detectors, which cover a larger angular range ($-10^\circ - 140^\circ$), and a much larger sample moderator distance (18 m), enabling higher resolution experiments. To fully explore the magnetic contribution to the INS spectrum, experiments were performed at a variety of incident energies (E_i) and temperatures (T), as shown in Table I. We have taken advantage of the nondispersive nature of CEF excitations and summed the signal in all detectors over a range of scattering angles ($5 < \phi < 45^\circ$) to improve the statistics of the data.

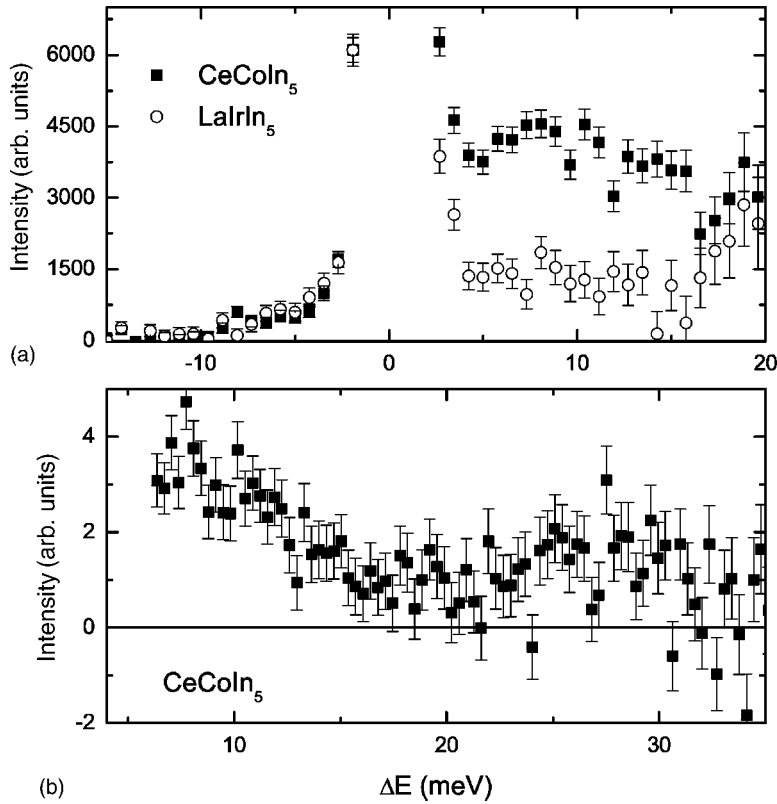


FIG. 1. (a) Inelastic neutron scattering spectra for CeCoIn_5 and LaIrIn_5 collected with PHAROS. Solid squares (open circles) indicate the spectrum for CeCoIn_5 (LaIrIn_5) collected at 18 K with $E_i=30.2$ meV. (b) Temperature dependence of the INS response of CeCoIn_5 . Shown is data collected at 80 K subtracted from data collected at 18 K with $E_i=48.5$ meV where the spectra at each temperature is normalized as described in the text.

We adopted two of the most frequently used methods to subtract the nonmagnetic scattering and extract the magnetic contribution to the INS spectra. Method one relies on subtracting the scattering observed in the nonmagnetic analog from that of the specified magnetic material. In this case the magnetic contribution $S_{mag}=S(\text{Ce},\text{SQ})-f S(\text{NM},\text{SQ})$, where SQ means small Q or low angle, NM means the nonmagnetic analog, and f is the ratio of the total scattering cross-section (σ) of the magnetic and nonmagnetic analog $\sigma(\text{Ce})/\sigma(\text{NM})$. For method two, the nonmagnetic analog is used to determine a scaling factor $R=S(\text{NM},\text{LQ})/S(\text{NM},\text{SQ})$ between the high and low angle data (LQ represents large Q or high angle data). This same factor is then used to scale the high angle data (where nonmagnetic scattering dominates) to small angles (where magnetic scattering dominates) in the Ce compound. (As variants on these methods, we also allow the factors f or R to be variable parameters in the least-squares fits to the CEF model.) In the results reported here, method one has been used. We will discuss the effect of different background subtractions further in Sec. IV.

To determine the CEF scheme and the effect of Kondo spin fluctuations, we have adopted both approaches discussed in the Introduction. In the first method we fit the magnetic contribution to the scattering to a CEF model for Ce^{3+} in a tetragonal environment. Several datasets for different incident energies and/or temperatures were fit simultaneously. The fitting variables were the CEF parameters (B_i^m 's), the width Γ_{ie} of the inelastic excitations (which are modeled as Lorentzians), and a scale factor for each dataset. We were unable to resolve a quasielastic contribution to the INS spectra. To prevent proliferation of fitting parameters,

we constrained the quasielastic width (Γ_{qe}) to be 1/4 of the inelastic width Γ_{ie} . For CeRhIn_5 (Ref. 27) and CeCoIn_5 (Ref. 25) this gives values of Γ_{qe} that are in good agreement with estimates from NMR experiments.²⁸ We then used the parameters derived from these fits in a calculation of the magnetic susceptibility χ_{CEF} . The CEF levels were treated as delta functions in energy and a mean field parameter λ was added to represent the Kondo effect at high temperatures.

In addition, we have carried out calculations for the Anderson impurity model for a $J=5/2$ impurity in the presence of CEF using the noncrossing approximation (NCA). As in Ref. 27, we have used a Gaussian background band with halfwidth (at half maximum) 2.5 eV, setting the $4f$ level 2 eV below the Fermi level and including a spin orbit splitting 0.273 eV of the $J=7/2$ states. The Kondo physics renormalizes the input CEF energies upwards by an amount approximately equal to $k_B T_K$, so the bare energies were chosen correspondingly smaller than those obtained from the CEF fits outlined above. The mixing parameter β [Eq. (2)] and the $4f$ -conduction electron hybridization parameter V were then chosen to give reasonable fits to both the INS spectra and to the measured susceptibility.

III. RESULTS AND ANALYSIS

We now present the results of INS on CeMIn_5 . We have made preliminary reports of some of these results elsewhere.^{25,27,29} For the $M=\text{Co}, \text{Ir}$ compounds we first present data that have been minimally processed in order to convey unambiguously the presence of magnetic scattering in the INS spectra. These data also serve as an indication of the uncertainty present in the measurements. (For CeRhIn_5

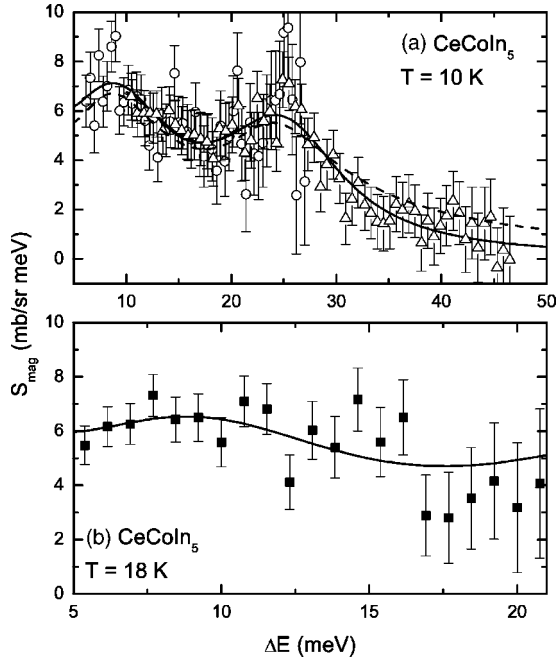


FIG. 2. S_{mag} for CeCoIn₅. (a) The open circles (triangles) indicate S_{mag} for data collected on LRMECS with $E_i=35$ and 60 meV, respectively, at 10 K. (b) Solid squares for data collected on PHAROS with $E_i=30.2$ meV at 18 K. In both (a) and (b) the solid line indicates a simultaneous fit to a CEF model. The dashed line in (a) is the result of an NCA calculation as described in the text.

similar data have been reported elsewhere.²⁷⁾ We then present the magnetic portion of the scattering as well as the results of least squares fits to the CEF model and representative NCA calculations.

A. CeCoIn₅

In Fig. 1(a), INS spectra collected on PHAROS for CeCoIn₅ is contrasted to that of LaIrIn₅ with $E_i=30.2$ meV at 18 K. The extra intensity in the INS spectra for CeCoIn₅ relative to the nonmagnetic analog LaIrIn₅ is attributed to CEF excitations in CeCoIn₅. Further evidence of CEF excitations in CeCoIn₅ is provided in Fig. 1(b). Here we use data that have *not* been corrected for neutron absorption or for the sample holder scattering. We subtract the data for $E_i=48.5$ meV at 80 K from that taken at 10 K. Each spectra has been normalized by the factor $n(\omega)+1=(1-\exp(-\hbar\omega/k_B T))^{-1}$ to account for the phonon population change with temperature. (This normalization only significantly affects the results at low energy transfers.) The fact that the difference shown in Fig. 1(b) is positive on the energy loss side of the spectrum is characteristic of the presence of CEF excitations. As the occupation of the ground state doublet decreases with increasing temperature, the amplitude of the excitation from the ground state to the excited states also decreases. We conclude that two broad CEF excitations centered at approximately 9 meV and 25 meV are present in the spectra for CeCoIn₅.

The magnetic part of the scattering, S_{mag} (method 1) is displayed for CeCoIn₅ in Fig. 2. The dependence of the mag-

TABLE II. CEF parameters for CeMIn₅. χ^2 is the reduced chi squared of the CEF model fits and the energy of the first (second) excited doublet is denoted by $E(\Gamma_7^2)$ ($E(\Gamma_6)$). The remainder of the parameters are as defined in the text. Except for χ^2 and β which are dimensionless and λ which is given in (mol/emu), all units are meV. In all three materials the groundstate is a Γ_7^1 , the first excited state a Γ_7^2 , and the second excited state is a Γ_6 . The numbers in square brackets are from the NCA calculations.

	CeRhIn ₅	CeCoIn ₅	CeIrIn ₅
χ^2	0.69	0.52	0.83
B_2^0	-1.03	-.81	-1.2
B_4^0	0.044	0.058	0.06
B_4^4	0.122	0.139	0.12
β [NCA]	0.60 [0.6]	0.86 [0.95]	0.70 [0.71]
Γ_{ie}	2.3	6.6	8.7
$E(\Gamma_7^2)$ [NCA]	6.9 [7]	8.6 [6.45]	6.7 [2]
$E(\Gamma_6)$ [NCA]	24 [25]	25 [21.44]	29 [22.56]
V	456	469	470
λ	35	40	70

netic form factor has been removed so that the spectra represent the $Q=0$ scattering. In Fig. 2(a) the open circles and triangles are for INS spectra collected at 10 K with LRMECS using $E_i=35$ and 60 meV. Note that there are two broad peaks in S_{mag} , which is consistent with the previous assessment of the data in Fig. 1. Figure 2(b) displays S_{mag} for $E_i=30.2$ meV collected at 18 K on PHAROS. In both Figs. 2(a) and 2(b) the solid line represents a simultaneous fit to the CEF model for all three datasets. The resulting CEF parameters and other pertinent parameters are summarized in Table II. These results indicate that Γ_7^1 is the ground state, Γ_7^2 is the first excited state, and the second excited state is Γ_6 . Due to the $\Delta J_z = \pm 1$ selection rule, the intensity of the peaks is sensitive to the degree of admixture of the $J_z=5/2$ and $3/2$ states in the Γ_7^1 and Γ_7^2 states. In particular, the strength of the 25 meV excitation ($\Gamma_7^1 \rightarrow \Gamma_6$) is proportional to β . The large widths of the inelastic excitations indicate the importance of strong Kondo spin fluctuations. In Fig. 3(a) we compare the measured magnetic susceptibility to the calculated value based on the CEF parameters determined from the INS data. The value of the mean field parameter λ , which accounts for the reduction of the susceptibility at high temperature due to the Kondo effect, is given in Table II. In Figs. 2(a) and 3(a) we also present the results of the NCA Anderson impurity calculation with input parameters given in Table II.

B. CeIrIn₅

INS spectra for CeIrIn₅ and LaIrIn₅ are presented in Fig. 4. In Fig. 4(a) the INS spectrum for CeIrIn₅ is shown along with that of LaIrIn₅ with $E_i=30.2$ meV at 18 K. The spectra have been corrected for monitor counts, sample mass, neutron absorption, and the contribution of the empty sample holder. Additional intensity is observed for CeIrIn₅ relative to LaIrIn₅, consistent with the presence of broadened CEF excitations in CeIrIn₅. As in CeCoIn₅, more detail is pro-

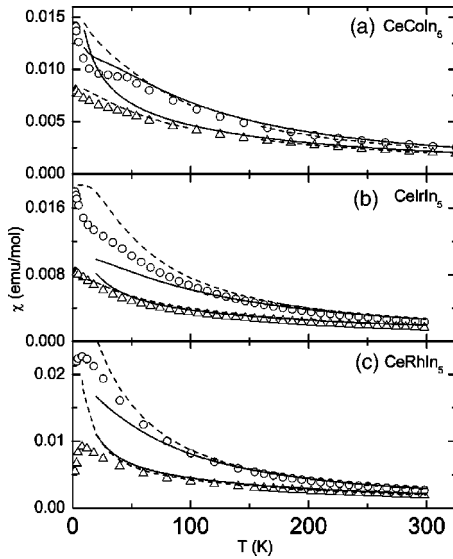


FIG. 3. The magnetic susceptibility for $CeMIn_5$. In all panels circles (triangles) represent χ_c (χ_{ab}) and solid (dashed) lines represent a CEF model fit (NCA calculations), respectively. The parameters of the fits are given in Table II.

vided upon examination of the temperature dependence of the scattering in $CeIrIn_5$. Figure 4(b) displays data, normalized as in Fig. 1(b), collected with $E_i=30.2$ meV at 70 K (PHAROS) and 80 meV at 100 K (LRMECS) subtracted from data taken at 18 K and 10 K, respectively. Here we use data that have *not* been corrected for neutron absorption or

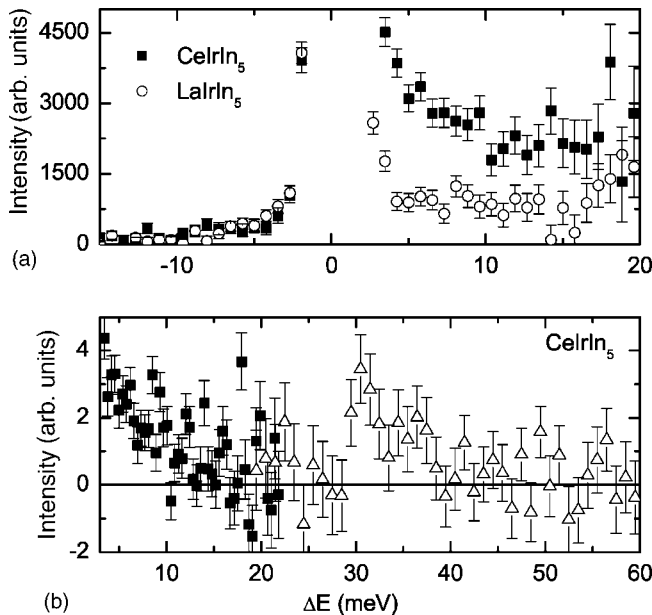


FIG. 4. (a) Inelastic neutron scattering spectra for $CeIrIn_5$ and $LaIrIn_5$ with $E_i=30.2$ meV at 18 K. Solid squares (open circles) indicate the spectrum for $CeIrIn_5$ ($LaIrIn_5$). (b) Temperature dependence of the INS response of $CeIrIn_5$. Shown is data collected at 70 K subtracted from data collected at 18 K with $E_i=30.2$ meV on PHAROS and data collected at 100 K subtracted from data collected at 10 K with $E_i=80$ meV on LRMECS where the spectra at each temperature is normalized as described in the text.

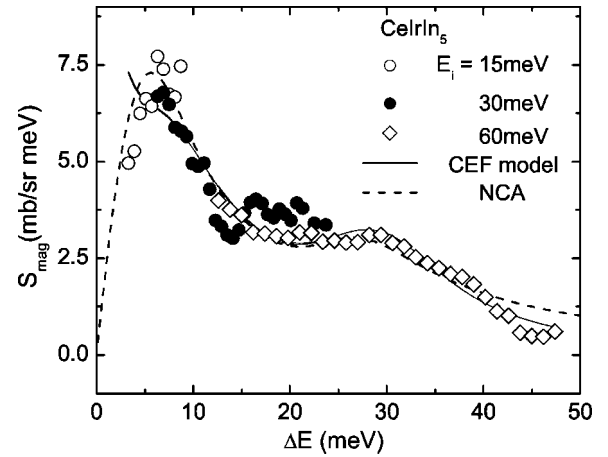


FIG. 5. S_{mag} for $CeIrIn_5$. The open circles, closed circles and open diamonds indicate S_{mag} for data collected at 10 K on LRMECS with $E_i=15, 30$ and 60 meV, respectively. The data have been smoothed for clarity. The solid line indicates a simultaneous fit to a CEF model. The dashed line is the result of an NCA calculation as described in the text.

for the empty holder scattering. Together, Figs. 4(a) and 4(b) indicate a broad CEF excitation centered in the 3–5 meV range and a second excitation near 30 meV.

The magnetic contribution to the INS spectra of $CeIrIn_5$ is displayed in Fig. 5. For clarity, the data have been smoothed. (Unsmoothed data as well as the magnetic part of the PHAROS INS spectra are reported in Ref. 29.) The symbols in Fig. 5 for three different E_i 's indicate two very broad peaks which are attributed to CEF excitations. The solid line in Fig. 5 is a fit to a CEF model, similar to the one previously presented for $CeCoIn_5$. The resulting parameters of this fit are summarized in Table II. As in the case of $CeCoIn_5$, Γ_7^1 is the ground state, Γ_7^2 is the first excited state, and the second excited state is Γ_6 . The CEF parameters also reproduce the high temperature magnetic susceptibility as shown in Fig. 3(b). The CEF splitting (6.7 meV) is somewhat smaller for the first excited state in $CeIrIn_5$ than in $CeCoIn_5$; however, Γ_{ie} is somewhat larger: 8.7 meV as compared to 6.6 meV for $CeCoIn_5$. The results of NCA calculations are included in Figs. 3(b) and 5 as dashed lines.

C. $CeRhIn_5$

Figure 6(a) shows the results of subtracting the data for $CeRhIn_5$ at 80 K from that taken at 10 K; CEF excitations are apparent at 7 and 25 meV. Figure 6(b) shows S_{mag} for $CeRhIn_5$. (We have obtained similar data with PHAROS which confirms the results of Ref. 27.) The 25 meV peak intensity is smaller relative to the 7 meV peak than in either $CeCoIn_5$ or $CeIrIn_5$. This indicates that $CeRhIn_5$ must have the least admixture of the $J_z=3/2$ state in the Γ_7^1 ground state. Note that the admixture of $J_z=3/2$ is not zero, since the peak intensity of the 25 meV excitation then would be identically zero and this is clearly not the case. The solid line in Fig. 6(b) indicates the best fit to a CEF model with parameters as summarized in Table II. The relative ordering of the wave functions is the same for $CeRhIn_5$ as for $CeCoIn_5$

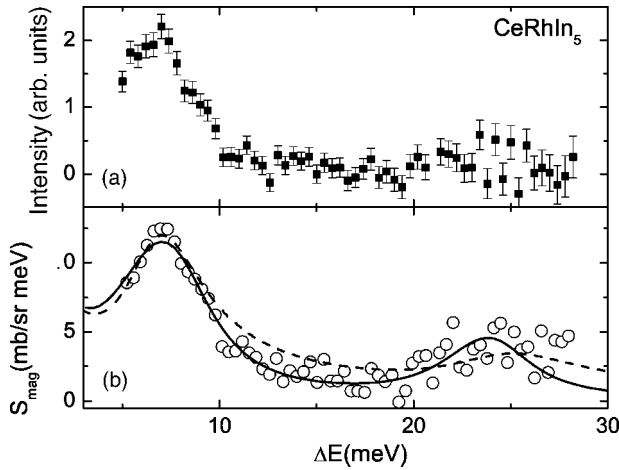


FIG. 6. (a) Temperature dependence of the INS response of CeRhIn₅. Shown is data collected at 100 K subtracted from data collected at 10 K with $E_i=35$ meV on LRMECS where the spectra at each temperature is normalized as described in the text. (b) The solid line indicates a simultaneous fit to a CEF model with $E_i=35$ meV at temperatures of 10, 70 and 140 K and $E_i=60$ meV at 10 K as described in Ref. 27. The dashed line in (b) is the result of an NCA calculation as described in the text.

and CeIrIn₅. The results of the NCA calculations are shown in Figs. 3(c) and 6(b).

IV. DISCUSSION

We first discuss the systematic errors in our determination of the CEF parameters. Because absorption is strong in these compounds, the signals are weak, and under these circumstances it is possible to overestimate the linewidth of broad peaks. Since the excitations in CeRhIn₅ and CeCoIn₅ are reasonably well-resolved, we do not think this is a problem. Hence we argue that the large observed linewidths, especially in CeIrIn₅, are not artifacts of the analysis but are real effects. Absorption also affects the estimate of the strength of the $\Gamma_7^1 \rightarrow \Gamma_6$ transition, since the final neutron energies are small for these larger energy transfers. Our absorption correction is based on a flat plate sample geometry and errors could arise from variation in sample thickness. This leads to an unknown uncertainty in our estimate of β . The determination of the nonmagnetic scattering also leads to systematic uncertainty. Methods discussed in Sec. II are reasonable but not rigorous. To estimate the resulting systematic uncertainty, we have examined the range of parameters obtained for all methods of nonmagnetic scattering subtraction. We find for all compounds that variations in β are small (± 0.05) and variations in $E[\Gamma_7^1 \rightarrow \Gamma_6]$ are of order ± 2 meV. Variations in $E[\Gamma_7^1 \rightarrow \Gamma_7^2]$ are small (± 0.2 meV) for CeRhIn₅, larger (± 1 meV) for CeCoIn₅ and largest for CeIrIn₅. Due to the large inelastic linewidth in CeIrIn₅, the excitations are not well resolved, so that values of $E[\Gamma_7^1 \rightarrow \Gamma_7^2]$ in the range 0–7 meV all give reasonable fits to the INS spectra and susceptibility. In all cases, the estimates of systematic error are larger than the statistical error. Consequently, error bars are not given in Table II.

The values we report in Table II can be viewed as representative, within these limits. They are obtained on the same spectrometers, under identical conditions, with identical methods of absorption correction and nonmagnetic background subtraction (method one). Hence, the results are consistent between the compounds and should accurately reflect trends in the CEF parameters. Our method of subtracting high temperature from low temperature raw data [Figs. 1(b), 4(b), and 6(a)] confirms that the positions of the peaks given in Table II are essentially correct. Further, the ratio of the $\Gamma_7^1 \rightarrow \Gamma_6$ peak intensity to that of the $\Gamma_7^1 \rightarrow \Gamma_7^2$ peak increases in the sequence M=Rh, Ir, Co which also confirms the trend seen in Table II that β increases in the same sequence. In addition, the calculations of the susceptibility based on the parameters of Table II adequately represent the magnitude and anisotropy of the susceptibility for $T > 50$ –100 K. These calculations include a single mean-field parameter λ that accounts for the reduction of the susceptibility by the Kondo effect (and also by antiferromagnetic correlations) at high temperatures. The values of T_K obtained from the assumption $\lambda = T_K/C_{5/2}$ are 28, 32 and 56 K for M=Rh, Co, Ir, respectively. These can be viewed as high temperature Kondo temperatures, in the regime where the excited states are occupied. As such, they are not only reasonable, but they also show the same trend as the inelastic linewidths, to which they should be proportional. Given all this, we believe that the values of excitation energies, mixing parameters and linewidths given in Table II are essentially correct, within the limits of systematic error.

The CEF parameters that we propose for CeMIn₅ are straightforwardly related to those of the parent compound CeIn₃. In CeIn₃, the ground state is a Γ_7 doublet, but the excited state at ~ 12 meV is a Γ_8 quartet.^{30–32} Upon lowering the cubic symmetry of CeIn₃ to the tetragonal symmetry of CeMIn₅, the 4-fold degeneracy of the Γ_8 quartet is lifted, resulting in the CEF level scheme consisting of three doublets as described in Sec. I. The ground state remains the Γ_7 (denoted as Γ_7^1 in tetragonal symmetry), but the value of β is no longer restricted to the value $\sqrt{5/6}$ required in cubic symmetry. For CeCoIn₅, the mixing parameter β remains close to the value that it has for cubic symmetry, but for the other two compounds, β deviates substantially. The quartet splits such that the first excited state is the Γ_7^2 doublet and the second excited state is the Γ_6 doublet.

We next address the issue of the uniqueness of the determination of the CEF parameters. We first note that experimental probes of CEF excitations are unable to differentiate between a positive and negative value of B_4^4 , i.e., only the moduli of the matrix elements are observable. Consequently, the distinction between the Γ_7^1 and Γ_7^2 states is a matter of convention. We have chosen Γ_7^1 as the ground state in analogy with the cubic case. There are two alternatives to our assignment of the Γ_6 doublet as the highest level. If the Γ_6 doublet were the ground state, B_2^0 would be positive. In tetragonal symmetry at high temperatures and in the absence of the Kondo effect or magnetic correlations, the parameter B_2^0 should be proportional to $(1/\chi_{ab}) - (1/\chi_c)$ ³³ and, hence, should be negative. If the Γ_6 were the first excited state, the strong peak intensity near 7 meV in CeRhIn₅ and the J_z

TABLE III. CEF level schemes (a comparison of all determinations). Δ_1 and Δ_2 represent the energy splitting between the groundstate and first and second excited states, respectively. The column corresponding to Order indicates the order of wave functions from the groundstate to the upper level. The column corresponding to β indicates the value for the groundstate wave function. Because of inconsistency in the literature with respect to the labeling of the wave functions, we have defined the wave functions as in Eq. (2).

Ref.	Δ_1 (meV)	Δ_2 (meV)	Order	β	Method
CeCoIn₅					
17 and 19	2.8	8.8	$\Gamma_6 \Gamma_7^1 \Gamma_7^2$	0.1	Mag. Susc., Spec. Heat and NMR
21	13	17	$\Gamma_7^1 \Gamma_7^2 \Gamma_6$	0.92	Mag. Susc. and Spec. Heat
22	13	14.3	$\Gamma_7^1 \Gamma_7^2 \Gamma_6$	0.519	Mag. Susc.
Present	8.6	25	$\Gamma_7^1 \Gamma_7^2 \Gamma_6$	0.86	INS
CeIrIn₅					
17	3.9	10.8	$\Gamma_7^1 \Gamma_6 \Gamma_7^2$	0.66	Mag. Susc. and Spec. Heat
20	5.3	25.9	$\Gamma_7^1 \Gamma_7^2 \Gamma_6$	0.213	Mag. Susc. and Therm. Expan.
Present	6.7	29	$\Gamma_7^1 \Gamma_7^2 \Gamma_6$	0.70	INS
CeRhIn₅					
17	6.0	12.1	$\Gamma_7^1 \Gamma_7^2 \Gamma_6$	≈ 0	Mag. Susc. and Spec. Heat
20	5.9	28.5	$\Gamma_7^1 \Gamma_7^2 \Gamma_6$	0.247	Mag. Susc. and Therm. Expan.
Present	6.9	24	$\Gamma_7^1 \Gamma_7^2 \Gamma_6$	0.60	INS

$= \pm 1$ selection rule would imply that the ground state is primarily $J_z=3/2$. However, this would imply that the second excited state is mostly $J_z=5/2$, so that there should be a strong amplitude for the transition to the upper level, contrary to the observed INS spectra. This basic situation is similar in CeIrIn₅ but is less clear in CeCoIn₅ where the amplitudes of both excited state peaks are comparable. However, because the CEF splitting in CeCoIn₅ is intermediate between that of CeIrIn₅ and CeRhIn₅ and because the susceptibility of the three compounds is essentially similar, the same CEF level scheme for all three cases is highly probable.

The results of all previous attempts to determine the CEF parameters in CeMIn₅ are summarized in Table III. The older results are based on susceptibility χ , specific heat C_v and thermal expansion α measurements and are relatively insensitive to the upper excitation Δ_2 because the CEF contributions to χ , C_v and α are small at the higher temperatures where this excitation becomes thermally populated. All three previous attempts at identifying the CEF level scheme in CeCoIn₅ identify a Γ_7^1 ground state, except for the case of Refs. 17 and 19. These latter authors identify a Γ_6 ground state and a positive value for B_2^0 . To account for this in their analysis of the magnetic susceptibility, a large and anisotropic mean field parameter was included. We think this is unlikely for the reasons given above. The results of Ref. 22 indicate a Γ_7^1 ground state; however, they find $\beta=0.519$, which indicates a larger admixture of the $J_z=5/2$ state into the ground state than determined here. They also find somewhat different energy splittings. The results of Ref. 21 show a similar β to that determined here, but minor differences in the value of the splittings. For CeIrIn₅ the value of β found in Ref. 20 is significantly different from that we find, though the excitation energies are in reasonable agreement. Apart from the sign convention, the ground state proposed in Ref. 17 is similar to the one proposed here; however, in that work the first excited state is a Γ_6 doublet and the energy of the second excited state is much smaller than reported here. All

previous attempts to determine the CEF level scheme in CeRhIn₅ agree on the relative ordering of the CEF levels. However, Refs. 17 and 20 propose such small values of β that the intensity of the second excited state would be considerably smaller than we observe. Moreover, for the small β proposed in Refs. 17 and 20, the calculated in-plane magnetic moment $g\mu_B\langle J_x \rangle$ is a factor of two smaller than the in-plane ordered moment observed by neutron diffraction ($0.75\mu_B$).³⁴ The in-plane moment ($0.92\mu_B$) calculated using the value of β that we propose is in better agreement with the observed value, and also suggests a moderate degree of moment reduction due to the Kondo effect.

We now turn to a discussion of the NCA calculations. It is clear from the broadness of the CEF excitations in CeMIn₅ that Kondo spin fluctuations play an essential role. However, only a modest increase in hybridization (Table II) is required to reproduce the observed changes in linewidths of the CEF excitations. For CeIrIn₅ the linewidth is sufficiently large that the first excited doublet cannot be resolved, and we find that we can fit the data assuming values of $E[\Gamma_7^1 \rightarrow \Gamma_7^2]$ in the range 0–7 meV. This means that the groundstate can be treated as a quartet. We note that the NCA calculations are unable to reproduce the low temperature features in the magnetic susceptibility. For this reason, and for the reason that we can find no set of CEF parameters which reproduces both the neutron data and the plateau in the *c*-axis magnetic susceptibility in CeCoIn₅, we believe that the feature must be due to correlations.²¹

Table II shows that there is no correlation between the magnitude of Δ_1 and the superconducting transition temperature, as suggested by recent theory.¹⁸ However, as the superconducting transition temperature increases so does the mixing parameter β . Moreover, an increase of level width (i.e., hybridization) correlates with the formation of the superconducting state as can be seen from the values of Γ_{ie} in Table II. A similar correlation is observed on comparison of CeCu₂Ge₂ (antiferromagnetic at 4.1 K³⁵) and CeCu₂Si₂ (su-

perconducting at 0.5 K³⁶): CeCu₂Si₂ has a larger Γ_{ie} than CeCu₂Ge₂ (Refs. 35 and 37) and tuning the hybridization of CeCu₂Ge₂ with applied pressure results in a superconducting transition of 0.64 at 101 kbar.³⁸ This also is consistent with the behavior of CeIn₃ under pressure¹⁶ where at ambient pressure Γ_{ie} for the CEF excitation in antiferromagnetic CeIn₃ (3 meV³²) is consistent with the value found in antiferromagnetic CeRhIn₅ (2.3 meV) rather than the much larger values of Γ_{ie} found in either of the ambient pressure superconductors CeCoIn₅ (6.6 meV) or CeIrIn₅ (8.7 meV). With the application of pressure, the hybridization in CeIn₃ is tuned, suppressing the antiferromagnetic order. The superconducting state is then formed near the QCP where antiferromagnetic order is suppressed. The evolution of the hybridization in CeMIn₅ indicates a similar picture where the substitution of a different transition metal is sufficient to change the hybridization. This suggests that CeCoIn₅, for which the superconducting transition temperature is highest and Γ_{ie} is fairly large, is near the QCP, while CeRhIn₅, which at ambient pressure is magnetically ordered and for which Γ_{ie} is relatively small, is on the magnetic side of the QCP. CeIrIn₅, where the superconducting transition temperature is lower and Γ_{ie} is larger than in CeCoIn₅, is slightly farther out on the nonmagnetic side of the QCP phase diagram. The QCP picture has been advocated by a number of previous authors.^{11–15}

V. CONCLUSIONS

We have measured the CEF excitations of the CeMIn₅ ($M=\text{Co, Rh, Ir}$) series of heavy fermion superconductors by

means of INS. The CEF excitations are broadened by the effect of Kondo spin fluctuations. Consequently, we have adopted two approaches to determine the CEF parameters, energy level splittings, and wave functions. The first approach fits the magnetic portion of the INS spectra by a CEF model where the peak widths are represented by a Lorentzian line shape. The second approach utilizes NCA calculations and represents a more sophisticated means of accounting for the effect of Kondo spin fluctuations. Both of these methods are able to reproduce the INS data and the magnetic susceptibility. Furthermore, these approaches yield a picture in which the CEF level splitting in all three materials is similar and can be thought of as being derived from the cubic parent compound CeIn₃ in which an excited state quartet is split into two doublets by the lower symmetry of the tetragonal environment of CeMIn₅. Although we find no correlation between the superconducting transition temperature and the level splitting, we do find a correlation between the f -conduction electron hybridization and the superconducting transition temperature where significant hybridization is required for the formation of the superconducting state.

ACKNOWLEDGMENTS

We acknowledge fruitful discussions with W. Bao and S. Kern. Work at Irvine was supported by the Department of Energy (DOE) under Grant No. DE-FG03-03ER46036. Work at Temple U. was supported by the DOE under Grant No. DE-FG02-01ER45827. Work at Los Alamos and Argonne was performed under the auspices of the DOE.

-
- ¹H. Hegger, C. Petrovic, E. G. Moshopoulou, M. F. Hundley, J. L. Sarrao, Z. Fisk, and J. D. Thompson, Phys. Rev. Lett. **84**, 4986 (2000).
- ²C. Petrovic, R. Movshovich, M. Jaime, P. G. Pagliuso, M. F. Hundley, J. L. Sarrao, Z. Fisk, and J. D. Thompson, Europhys. Lett. **53**, 354 (2001).
- ³C. Petrovic, P. G. Pagliuso, M. F. Hundley, R. Movshovich, J. L. Sarrao, J. D. Thompson, Z. Fisk, and P. Monthoux, J. Phys.: Condens. Matter **13**, L337 (2001).
- ⁴J. D. Thompson, M. Nicklas, A. Bianchi, R. Movshovich, A. Llobet, W. Bao, A. Malinowski, M. F. Hundley, N. O. Moreno, P. G. Pagliuso, J. L. Sarrao, S. Nakatsuji, Z. Fisk, R. Borth, E. Lengyel, N. Oeschler, G. Sparn, and F. Steglich, Physica B **329–333**, 446 (2003).
- ⁵S. Kawasaki, T. Mito, Y. Kawasaki, G.-q. Zheng, Y. Kitaoka, D. Aoki, Y. Haga, and Y. Onuki, Phys. Rev. Lett. **91**, 137001 (2003).
- ⁶R. Movshovich, M. Jaime, J. D. Thompson, C. Petrovic, Z. Fisk, P. G. Pagliuso, and J. L. Sarrao, Phys. Rev. Lett. **86**, 5152 (2001).
- ⁷R. A. Fisher, F. Bouquet, N. E. Phillips, M. F. Hundley, P. G. Pagliuso, J. L. Sarrao, Z. Fisk, and J. D. Thompson, Phys. Rev. B **65**, 224509 (2002).
- ⁸G.-q. Zheng, K. Tanabe, T. Mito, S. Kawasaki, Y. Kitaoka, D. Aoki, Y. Haga, and Y. Onuki, Phys. Rev. Lett. **86**, 4664 (2001).
- ⁹Y. Kohori, Y. Yamato, Y. Iwamoto, T. Kohara, E. D. Bauer, M. B. Maple, and J. L. Sarrao, Phys. Rev. B **64**, 134526 (2001).
- ¹⁰T. Mito, S. Kawasaki, G.-q. Zheng, Y. Kawasaki, K. Ishida, Y. Kitaoka, D. Aoki, Y. Haga, and Y. Onuki, Phys. Rev. B **63**, 220507(R) (2001).
- ¹¹M. Nicklas, R. Borth, E. Lengyel, P. G. Pagliuso, J. L. Sarrao, V. A. Sidorov, G. Sparn, F. Steglich, and J. D. Thompson, J. Phys.: Condens. Matter **13**, L905 (2001).
- ¹²J. S. Kim, J. Alwood, G. R. Stewart, J. L. Sarrao, and J. D. Thompson, Phys. Rev. B **64**, 134524 (2001).
- ¹³V. A. Sidorov, M. Nicklas, P. G. Pagliuso, J. L. Sarrao, Y. Bang, A. V. Balatsky, and J. D. Thompson, Phys. Rev. Lett. **89**, 157004 (2002).
- ¹⁴J. Paglione, M. A. Tanatar, D. G. Hawthorn, E. Boaknin, R. W. Hill, F. Ronning, M. Sutherland, L. Taillefer, C. Petrovic, and P. C. Canfield, Phys. Rev. Lett. **91**, 246405 (2003).
- ¹⁵A. Bianchi, R. Movshovich, I. Vekhter, P. G. Pagliuso, and J. L. Sarrao, Phys. Rev. Lett. **91**, 257001 (2003).
- ¹⁶N. D. Mathur, F. M. Grosche, S. R. Julian, I. R. Walker, D. M. Freye, R. K. W. Haselwimmer, and G. G. Lonzarich, Nature (London) **394**, 39 (1998).
- ¹⁷P. G. Pagliuso, N. J. Curro, N. O. Moreno, M. F. Hundley, J. D. Thompson, J. L. Sarrao, and Z. Fisk, Physica B **320**, 370 (2002).
- ¹⁸T. Takimoto, T. Hotta, T. Maehira, and K. Ueda, J. Phys.: Con-

- dens. Matter **14**, L369 (2002).
- ¹⁹N. J. Curro, B. Simovic, P. C. Hammel, P. G. Pagliuso, J. L. Sarrao, J. D. Thompson, and G. B. Martins, Phys. Rev. B **64**, 180514 (2001).
- ²⁰T. Takeuchi, T. Inoue, K. Sugiyama, D. Aoki, Y. Tokiwa, Y. Haga, K. Kindo, and Y. Onuki, J. Phys. Soc. Jpn. **70**, 877 (2001).
- ²¹S. Nakatsuji, S. Yeo, L. Balicas, Z. Fisk, P. Schlottmann, P. G. Pagliuso, N. O. Moreno, J. L. Sarrao, and J. D. Thompson, Phys. Rev. Lett. **89**, 106402 (2002).
- ²²H. Shishido, R. Settai, D. Aoki, S. Ikeda, H. Nakawaki, N. Nakamura, T. Iizuka, Y. Inada, K. Sugiyama, T. Takeuchi, K. Kindo, T. C. Kobayashi, Y. Haga, H. Harima, Y. Aoki, T. Namiki, H. Sato, and Y. Onuki, J. Phys. Soc. Jpn. **71**, 162 (2002).
- ²³G. Fischer and A. Herr, Phys. Status Solidi B **141**, 589 (1987).
- ²⁴E. G. Moshopoulou, Z. Fisk, J. L. Sarrao, and J. D. Thompson, J. Solid State Chem. **158**, 25 (2001).
- ²⁵E. D. Bauer, A. D. Christianson, J. M. Lawrence, E. A. Goremychkin, N. O. Moreno, N. J. Curro, F. R. Trouw, J. L. Sarrao, J. D. Thompson, R. J. McQueeney, W. Bao, and R. Osborn, J. Appl. Phys. **95**, 7201 (2004).
- ²⁶J. M. Lawrence, R. Osborn, J. L. Sarrao, and Z. Fisk, Phys. Rev. B **59**, 1134 (1999).
- ²⁷A. D. Christianson, J. M. Lawrence, P. G. Pagliuso, N. O. Moreno, J. L. Sarrao, J. D. Thompson, P. S. Riseborough, S. Kern, E. A. Goremychkin, and A. H. Lacerda, Phys. Rev. B **66**, 193102 (2002).
- ²⁸N. J. Curro, J. L. Sarrao, J. D. Thompson, P. G. Pagliuso, S. Kos, A. Abanov, and D. Pines, Phys. Rev. Lett. **90**, 227202 (2003).
- ²⁹A. D. Christianson, J. M. Lawrence, P. S. Riseborough, N. O. Moreno, P. G. Pagliuso, E. D. Bauer, J. L. Sarrao, W. Bao, E. A. Goremychkin, S. Kern, F. R. Trouw, and M. P. Hehlen, cond-mat/0402020; J. Neutron Res. (to be published).
- ³⁰A. M. Van Diepen, R. S. Craig, and W. E. Wallace, J. Phys. Chem. Solids **32**, 1867 (1971).
- ³¹J. M. Lawrence and S. M. Shapiro, Phys. Rev. B **22**, 4379 (1980).
- ³²A. P. Murani, A. D. Taylor, R. Osborn, and Z. A. Bowden, Phys. Rev. B **48**, 10606 (1993).
- ³³P. Boutron, Phys. Rev. B **7**, 3226 (1973).
- ³⁴W. Bao, P. G. Pagliuso, J. L. Sarrao, J. D. Thompson, Z. Fisk, J. W. Lynn, and R. W. Erwin, Phys. Rev. B **62**, R14621 (2000); **67**, 099903(E) (2003).
- ³⁵G. Knopp, A. Loidl, K. Knorr, L. Pawlak, M. Duczmal, R. Caspary, U. Gottwick, H. Spille, F. Steglich, and A. P. Murani, Z. Phys. B: Condens. Matter **77**, 95 (1989).
- ³⁶F. Steglich, J. Aarts, C. D. Bredl, W. Lieke, D. Meschede, W. Franz, and H. Schafer, Phys. Rev. Lett. **43**, 1892 (1979).
- ³⁷E. A. Goremychkin and R. Osborn, Phys. Rev. B **47**, 14280 (1993).
- ³⁸D. Jaccard, K. Behnia, and J. Sierro, Phys. Lett. A **163**, 475 (1992).